Influence of organic semiconductor-metal interfaces on the photoresponse of functionalized anthradithiophene thin films

J. Day,[1] A. D. Platt,[1] S. Subramanian,[2] J. E. Anthony,[2] and O. Ostroverkhova[1,a)]
[1]*Oregon State University, Corvallis, Oregon 97331, USA*
[2]*University of Kentucky, Lexington, Kentucky 40506, USA*

(Received 10 October 2008; accepted 8 April 2009; published online 22 May 2009)

We report on the contribution of effects at the organic semiconductor-metal interfaces to dark current and to transient and continuous wave (cw) photocurrent in high-performance functionalized anthradithiophene (ADT) films deposited from solution on glass substrates with gold (Au) and aluminum (Al) electrodes. In all samples, fast sub-30 ps charge carrier photogeneration was observed under photoexcitation with 100 fs, 400 nm laser pulses. Amplitudes of the transient photocurrent measured in samples with Au and Al electrodes were similar within a factor of 2–4, depending on the sample and on the applied voltage. Compared to transient photocurrents, dark currents, and cw photocurrents exhibited pronounced differences between ADT films on Au and Al electrodes, with considerably higher currents in samples with Au electrodes. Measurements of photoresponse under uniform illumination were complemented by scanning photocurrent microscopy performed on the same samples. Photocurrent profiles were obtained by scanning the gap between coplanar electrodes with a tightly focused beam, either pulsed or cw, and measuring photocurrent, either transient or steady-state at every point. While samples with Au and Al electrodes exhibited similar distributions of the transient photocurrent amplitudes in the gap, those of the cw photocurrents exhibited dramatic differences, in agreement with results obtained under uniform illumination. © *2009 American Institute of Physics*. [DOI: 10.1063/1.3129693]

I. INTRODUCTION

Organic semiconducting materials, in order to be used in (opto)electronic applications, must be integrated into device structures in which they are interfaced with inorganic materials, often metals. Therefore, processes occurring at such interfaces and their influence on the device performance are of great interest.[1–3] In particular, it is important to distinguish the part played by carrier dynamics in bulk material from that played by interface dynamics, so that the contribution of each to the behavior of the overall system may be understood. Such questions are by no means fully answered at the present time.[1]

One of the materials classes promising for low-cost (opto)electronic applications are high-performance solution-processable small-molecular-weight organic semiconductors. Recently, significant progress has been made in synthesis and fabrication of thin-film devices based on such materials, in particular, functionalized pentacene and anthradithiophene (ADT) derivatives.[4–10] Charge carrier mobilities of over 1.2 $cm^2/(V\,s)$ have been demonstrated in thin-film-transistors (TFTs) based on drop-cast and spin-coated films of pentacene functionalized with triisopropylsilylethynyl (TIPS) groups[5] and of fluorinated ADT functionalized with triethylsilylethynyl (TES) groups,[8] respectively. The latter derivative is one of the two functionalized ADT derivatives studied here in device structures with gold (Au) and with aluminum (Al) electrodes.

Theoretically, ohmic, neutral, and blocking contacts can be distinguished, depending on their ability to inject charge carriers in the semiconductor.[11,12] In practice, however, it is not easy to unambiguously determine the nature of the contact.[3] Also, creating a specific type of contact on demand could be challenging. A need for contacts of different kinds may arise depending on the material and on the type of the measurement or application. For example, in measurements of charge carrier mobility using the time-of-flight technique, blocking contacts are necessary,[13] whereas ohmic contacts are desirable in TFT structures.[14] The choice of the best contacts to use when characterizing photoconductive properties of materials could be difficult.[15,16] For instance, while blocking contacts would ensure low dark current and low contamination of the bulk material with trapped injected charges, they can prevent effective extraction of photoexcited carriers, which would lead to charge accumulation at the interfaces; thereby screen electric field in the film and limit photoresponse. If ohmic contacts are used, however, the material can become charged due to extensive trapping of charge carriers injected from the electrodes, followed by space-charge field formation, which might skew the results of the measurements of intrinsic photoconductivity. Optimization of photoconductive performance of planar devices (e.g., photodetectors,[17] photorefractive devices,[18,19] etc.) could represent an additional challenge due to non-uniform electric field distribution across the channel. In this paper, we seek to explore the influence of the effects mentioned above on the photoresponse of high-performance functionalized ADT derivatives in planar device structures with either blocking (Al) or near-Ohmic (Au) contacts. Dark currents, continuous wave (cw) photocurrent and transient photoresponse with sub-30 ps time resolution were measured, and related to the

a)Electronic mail: oksana@science.oregonstate.edu.

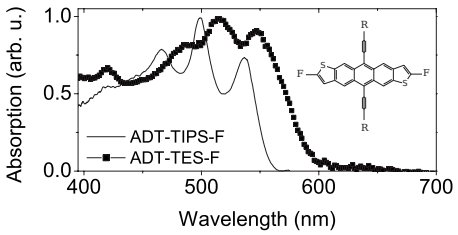

FIG. 1. Typical optical absorption spectra of ADT-TIPS-F and ADT-TES-F films. Inset shows molecular structures [$R=\mathrm{Si}(i-\mathrm{Pr})_3$ in ADT-TIPS-F, and $R=\mathrm{Si}(\mathrm{Et})_3$ in ADT-TES-F].

photocurrent profiles obtained by scanning the gap between coplanar electrodes with a tightly focused beam (either pulsed or cw) and measuring photocurrent (either transient or steady-state) at every point.

II. MATERIALS

The materials used in our study are fluorinated ADT derivatives, functionalized with TIPS or TES side-groups[4,6] (ADT-TIPS-F or ADT-TES-F, respectively, inset of Fig. 1). Both derivatives exhibit brick-wall-type crystal packing, with significant π-overlap.[4,6] ADT-TES-F has been recently explored in TFT applications: high-quality spin-coated polycrystalline films were obtained, with TFT hole mobilites ranging between 0.01 and ~1.5 $\mathrm{cm}^2/(\mathrm{V\ s})$, depending on the film deposition conditions and treatment of the electrodes.[6,8–10] In ADT-TIPS-F films, photocurrent at various time-scales after photoexcitation has been recently studied as a function of applied electric field, temperature, wavelength, light intensity, etc.[7] At room temperature, steady-state cw photoresponse in ADT-TIPS-F films was considerably higher than that in functionalized pentacene polycrystalline films[7,20–22] and in dicyanomethylenedihydrofuran glasses (used in photorefractive applications[19]).

Glass substrates were prepared by photolithographic deposition of 100-nm-thick Al or Cr (5 nm)/Au (50-nm)-thick electrode pairs. Pairs were fabricated in two configurations, the first consisting of ten interdigitated finger-pairs, with 1 mm finger length, 25 μm finger width and 25 μm gaps between the fingers of opposite electrodes, the second consisting of six finger-pairs, with the same length and spacing, but with 50 μm finger width. Coplanar pairs, with either 25 or 50 μm gap were also prepared. Au and Al (with work functions of 5.1 and 4.2 eV, respectively[3]), interfaced with the ADT derivatives [with highest occupied molecular orbital (HOMO) and lowest unoccupied molecular orbital energy levels of 5.35 and 3.07 eV, respectively, as measured by differential pulse voltammetry[23,24]], make hole-injecting and blocking contacts, respectively, thus creating very different charge injection conditions. ADT-TIPS-F and ADT-TES-F polycrystalline films with thicknesses of 0.5–2 μm were drop-cast from 3 wt % solution in toluene onto the substrates at ~60 °C in air. At least five samples of each material on each metal type and of each configuration of electrodes were prepared. Films deposited under inert atmosphere on the substrates precleaned in sulphuric acid were also tested and yielded similar results. Typical optical absorption spectra of ADT-TIPS-F and ADT-TES-F films are shown in Fig. 1. ADT-TIPS-F and ADT-TES-F exhibited identical absorption spectra in toluene solution,[23] but differed in the solid state: spectra of ADT-TES-F films were red-shifted with respect to those of ADT-TIPS-F films. This shift, observed regardless of possible sample-to-sample variation in film morphologies,[23] is most likely due to differences in molecular packing of ADT-TES-F and ADT-TIPS-F in a solid.[6]

III. EXPERIMENTAL

A. Transient and cw photoresponse and dark current

For transient photocurrent measurements, an amplified Ti:sapphire laser (800 nm, 100 fs, and 1 kHz) was used in conjunction with a frequency-doubling beta-barium borate crystal to excite the samples at a wavelength of 400 nm. Fluences in the 10–100 $\mu\mathrm{J}/\mathrm{cm}^2$ range were used. Voltage in the range of 10–150 V was supplied by a Keithley 237 source-measure unit and laser-pulse-induced transient photocurrent (I_{ph}) was measured with a 50 Ω load resistor by a 50 GHz Tektronix CSA8200 digital sampling oscilloscope (DSO) with time resolution of about 30 ps.[7]

In the measurements of cw photoresponse, the sample was excited by a $\mathrm{Nd}:\mathrm{YVO}_4$ laser at the wavelength of 532 nm. The Keithley 237 source-measure unit was used to measure dark current (I_d) and current under cw illumination either point-by-point or by performing voltage sweeps, from 0 to a maximum of 300 V. For measurements of temperature dependencies, the samples were embedded in a fixture incorporating thermoelectric unit for temperature control in the 285–330 K range. The cw photocurrent (I_{cw}) was calculated as the difference between the current under illumination and dark current. The light intensities were kept below 1 $\mathrm{mW}/\mathrm{cm}^2$, except in measurements of light intensity dependence of the cw photocurrent, in which the intensity was varied between 0.5 and 25 $\mathrm{mW}/\mathrm{cm}^2$.

In most of our experiments, the samples were (uniformly) illuminated from the glass substrate side, to minimize photoinjection and photoemission effects by the electrodes.[25,26] However, data were also taken with illumination from the film side and compared with data taken with illumination from the glass substrate side, to assess the contribution of such effects, as well as those of glass-organic film and organic film-air interfaces. No such contributions were detected in either transient or cw photoresponse.

B. Scanning photocurrent microscopy

Scanning photocurrent microscopy has been previously utilized to probe internal electric field distributions, map electronic band structure, measure mobility-lifetime products, etc. in inorganic and organic films, nanowires, carbon nanotubes, and graphene sheets.[17,27–31] In our experiments, ADT films on coplanar electrodes, either Al or Au, separated by a 50 μm gap, were excited with a focused beam from the glass substrate side, and photoresponse was monitored as the excitation spot was moved across the gap from one electrode to another (Fig. 2), under applied voltage. This experiment was performed with either pulsed 100 fs 400 nm excitation or cw 532 nm excitation, using laser sources described

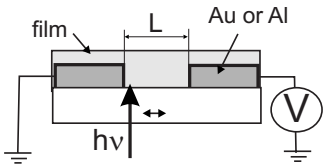

FIG. 2. Schematics of the scanning photocurrent microscopy experiment.

above. In the case of pulsed excitation, a lens with 2.5 cm focal distance was used to focus the beam with pulse energy of ~1 nJ to an approximately 4 μm spot at the sample. The lens was translated along the gap using a micrometer-controlled translation stage. At each position of the lens, transient photocurrent resulting from excitation of a localized region of the film was recorded with the DSO. In the case of cw excitation, the sample was placed under Olympus IX-71 inverted microscope, and a 10× objective with a numerical aperture of 0.6 was used to focus the beam at the power of ~0.4 μW to an approximately 400 nm spot. Position of the localized excitation with respect to the electrodes was monitored by a charge coupled device (CCD) camera that detected fluorescence (emitted by the photoexcited region of the sample) collected through the same objective. The sample was translated using a closed-loop piezoelectrically controlled *x-y* stage with sub-nanometer resolution, with a speed of 1 μm/s. Cw light was chopped at 565 Hz, and the amplitude of the modulated photocurrent signal was measured by a Stanford Research Systems 830 lock-in amplifier. The experiment was repeated as a function of applied voltage and light power, as well as at different voltage polarities, directions of the scan, and lengths of the waiting period between the successive scans.

IV. RESULTS

A. Transient photocurrent

Transient photocurrents with a rise time of several tens of picoseconds, limited by the time resolution of our setup,[7] were observed in both ADT-TIPS-F and ADT-TES-F films, regardless of the electrode material or geometry. The shapes of the transients were similar in ADT-TIPS-F and ADT-TES-F films and could be characterized by a fast initial decay (due to initial charge trapping and recombination) followed by a slower decay component (due to detrapping, transport, and recombination of the previously trapped carriers) that lasted up to at least tens of microseconds.[23,24] Figure 3(a) shows transient photocurrents, normalized at their peak values and measured in ADT-TIPS-F films on Au and Al electrodes. Interestingly, the faster decay component was more pronounced in films on Al electrodes, whereas the slower one was independent of the electrode material and could be described by a power-law function ($I_{ph} \sim t^{-\beta}$) with $\beta \sim 0.2-0.3$ in ADT-TES-F and 0.4–0.6 in ADT-TIPS-F [inset of Fig. 3(a)] over several orders of magnitude in time.[7,20,21,23,24,32] In samples with a 25 μm gap at voltages above ~30 V, the difference in the peak transient amplitudes for films on Au and films on Al electrodes was comparable to that due to morphology-related sample-to-sample variation[7] of approximately a factor of 2 [Fig. 3(b)]. The

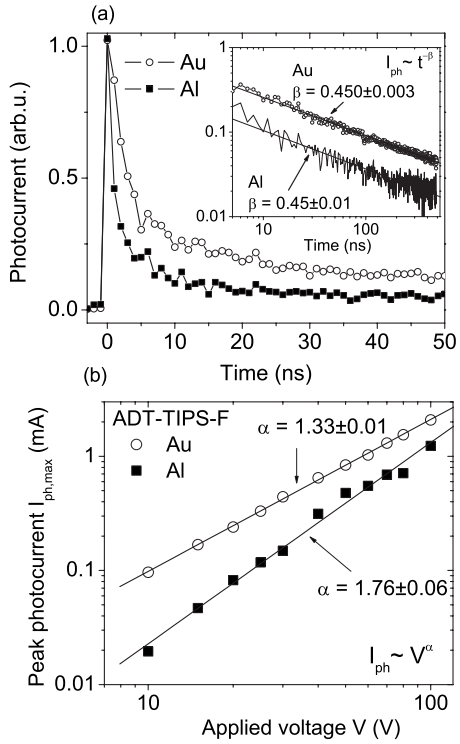

FIG. 3. (a) Transient photocurrents, normalized at their peak values, obtained in ADT-TIPS-F films on Au and Al electrodes under the same experimental conditions. Inset: long time-scale dynamics of the same transient photocurrents. Power-law fits ($I_{ph} \sim t^{-\beta}$) are also shown. (b) Transient photoresponse peak amplitude ($I_{ph,max}$) as a function of applied voltage obtained in ADT-TIPS-F samples with Al or Au interdigitated electrodes.

amplitude of the photocurrent ($I_{ph,max}$) is given by $I_{ph,max} = eN_{ph}\eta\mu Ed$, where e is the charge of the electron, N_{ph} is the number of absorbed photons per area per pulse, η is the photogeneration efficiency, E is the electric field, and d is the length of the electrode (i.e., the width of the channel). Here, μ is a sum of hole and electron mobilities which is dominated by hole mobility in our materials.[6] The photogeneration efficiency η includes carrier loss due to initial trapping and recombination within the first several tens of picoseconds, not resolved in our experiment (i.e., $\eta < \eta_0$, where η_0 is the initial photogeneration efficiency).[7] The average electric field E_{av} is given by $E_{av} = V/L$, where V is the applied voltage and L is the gap between the electrodes. However, since the electric field is not uniform in semiconductor devices with planar electrode geometry,[18] as discussed in Sec. V, and may be strongly affected by the electrode material, the data throughout Sec. IV will be presented as a function of applied voltage (V), rather than electric field E, to avoid ambiguity. The relation between the peak amplitude and applied voltage ($I_{ph,max} \sim V^{\alpha}$) was sample-dependent, with $\alpha \sim 1.3-1.8$.[7] Analysis of the behavior of many samples; however, yielded that on average, α in samples with Al electrodes was higher than in those with Au electrodes [e.g., $\alpha = 1.76 \pm 0.06$ and 1.33 ± 0.01 in ADT-TIPS-F films on Al and Au electrodes, respectively, in Fig. 3(b)]. Similar dependencies were observed for all electrode geometries, regardless of film-side or glass substrate-side illumination.

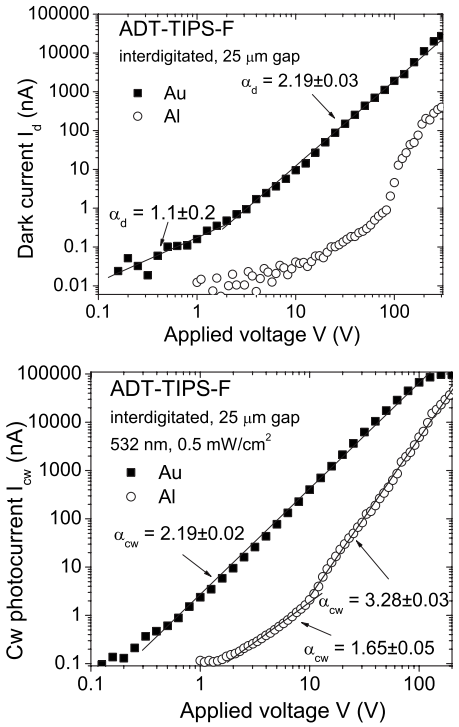

FIG. 4. (a) Dark current (I_d) and (b) cw photocurrent (I_{cw}) obtained in ADT-TIPS-F films with Al and Au contacts in interdigitated geometry with 25 μm gap. Power-law fits $I_d \sim V^{\alpha_d}$ and $I_{cw} \sim V^{\alpha_{cw}}$ in (a) and (b), respectively, are also shown.

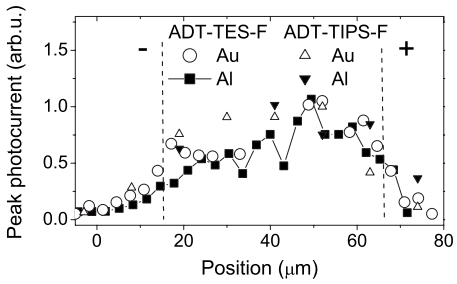

FIG. 5. Peak amplitudes of the transient photocurrent, normalized at their maximal values in the gap, at different positions of the localized beam spot obtained in ADT-TES-F and ADT-TIPS-F films on Au and Al electrodes, in coplanar electrode geometry with 50 μm gap at 100 V and 150 V, respectively. Dashed lines correspond to the geometrical edges of the electrodes.

B. Dark current and cw photocurrent

Unlike the amplitudes of transient photocurrent, the cw photocurrents (I_{cw}) and dark currents (I_d) for films on Au and on Al electrodes differed by more than an order of magnitude over a wide range of applied voltages, with much higher currents measured in samples with Au electrodes (Fig. 4). Voltage dependencies of the dark current and of the cw photocurrent observed in samples with Au and Al electrodes were drastically different, indicative of different mechanisms responsible for observed currents, depending on the electrode material. In samples with Au electrodes, the relationship between dark current and voltage ($I_d \sim V^{\alpha_d}$) was close to linear at very low voltages and close to quadratic at higher voltages [e.g., $\alpha_d = 1.1 \pm 0.2$ at voltages below 2 V and 2.19 ± 0.03 from 2 to 300 V in an ADT-TIPS-F film in Fig. 4(a)]. In contrast, in samples with Al electrodes, dark current was weakly voltage-dependent at lower voltages, followed by a steep increase at higher voltages. Despite this sharp increase, even at the highest applied voltage of 300 V used in our experiments, dark current in samples with Al electrodes was much lower than that in samples with Au electrodes at the same voltage. In films on either Au or Al electrodes, the cw photocurrent was higher than the dark current in the entire range of light intensities used. Regardless of the material, in samples with Au electrodes, α_{cw} obtained from the fit of voltage dependence of the photocurrent ($I_{cw} \sim V^{\alpha_{cw}}$) ranged between 1.5 and 2.2, depending on the sample. In any given sample, however, a single value of α_{cw} was sufficient to describe voltage dependence of the cw photocurrent over a large voltage range [e.g., $\alpha_{cw} = 2.19 \pm 0.02$ from 0.5 to 100 V in an ADT-TIPS-F film in Fig. 4(b)]. In samples with Al electrodes, however, α_{cw} was $\sim 1.3-3$ at lower voltages [e.g., $\alpha_{cw} = 1.65 \pm 0.05$ in Fig. 4(b)], depending on the sample, followed by steep transition described by $\alpha_{cw} \sim 3.3-5$ [e.g., $\alpha_{cw} = 3.28 \pm 0.03$ in Fig. 4(b)] at higher voltages. ADT films on Au and Al electrodes exhibited different dependencies of cw photocurrent (I_{cw}) on light intensity (I). In particular, the intensity dependence of cw photoresponse ($I_{cw} \sim I^b$) in samples with Au electrodes was weak, with $b \sim 0.2-0.3$, which suggests saturation of the current flow the film can support. In samples with Al electrodes, the intensity dependence was stronger, with $b \sim 0.6-0.7$, in the range of $0.5 < b < 1$ typically attributed to shallow trapping.[7,34]

C. Scanning photocurrent microscopy

1. Transient photocurrent

The peak amplitudes of the transient photocurrent measured at different positions of the localized pulsed photoexcitation (Sec. III B) of ADT-TES-F and ADT-TIPS-F films on Au and Al electrodes are shown in Fig. 5. No signal was detected at any position in the absence of applied voltage. Change in the transient photocurrent amplitude upon scanning of the pulsed focused beam across a planar device has been previously related to internal electric field distribution in InP planar devices.[30] In ADT films, although the exact distribution of transient photocurrent amplitudes in the gap somewhat depended on the measurement protocol (such as direction of the scan and waiting time between the data points), these distributions in samples with Au and Al electrodes were similar within the experimental error and, with our spatial resolution, relatively uniform across the gap. In particular, the amplitudes of transient photocurrents obtained upon excitation of near-electrode regions and of a midgap region were within a factor of 2 of each other. Transient photocurrent decay dynamics under localized excitation in samples with Au and Al electrodes were similar to those in Fig. 3(a) obtained under uniform illumination, with the initial decay faster in samples with Al electrodes. No dependence of the decay dynamics of the transient photocurrent on the beam position in the gap was observed.

2. Cw photocurrent

Figures 6(a) and 6(b) show the cw photoresponse measured under localized excitation of ADT-TIPS-F films on Al

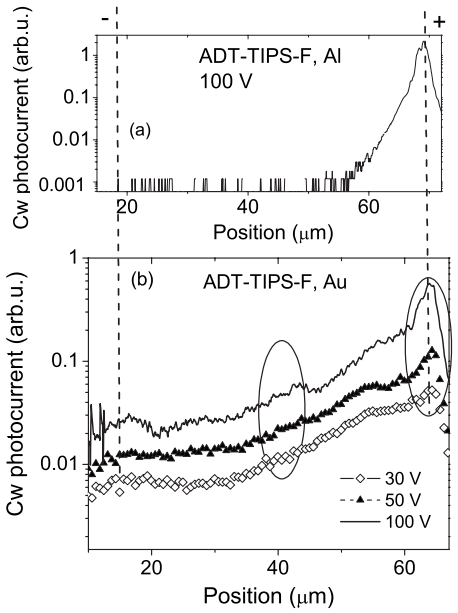

FIG. 6. Cw photoresponse as a function of the beam position obtained in an ADT-TIPS-F film in coplanar electrode geometry with 50 μm gap with (a) Al electrodes at 100 V and (b) Au electrodes at 30, 50, and 100 V. In (b), the curves are shifted along y-axis for clarity. Ovals denote the "midgap" and "near-the-positively biased-electrode" regions, more data for which are shown in Fig. 7. Vertical dashed lines show positions of the edges of the electrodes.

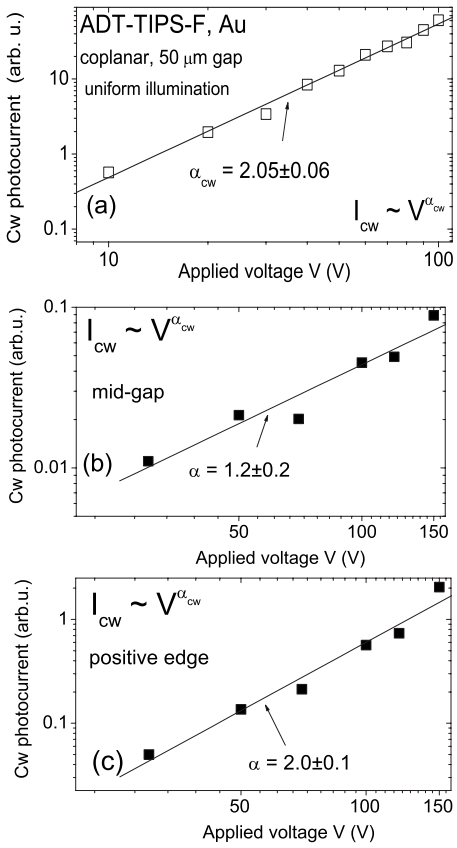

FIG. 7. Cw photoresponse obtained in an ADT-TIPS-F film in coplanar electrode geometry with 50 μm gap with Au electrodes under (a) uniform illumination and (b) and (c) localized excitation of (b) midgap region and (c) of a region close to positive electrode (denoted by ovals in Fig. 6). Fits with a power-law function $I_{cw} \sim V^{\alpha_{cw}}$ are also shown.

and Au electrodes, respectively, as a function of the beam position in the gap. Samples with either Al or Au electrodes showed a marked peak in photoresponse at the excitation near the positively biased electrode, which became more pronounced as the voltage increases. This effect was independent of the direction of the scan and was observed at all light powers ranging between 0.03 and 4 μW used in our experiments. As seen from Fig. 6(a), at 100 V, in the case of Al electrodes, photoresponse was mostly limited to the several micron-wide regions. Under the same conditions, photoresponse in the sample with Au electrodes was more uniform within the gap [Fig. 6(b)], yielding measurable photocurrents upon excitation of the midgap region, as well as of the region close to the negatively biased electrode. Interestingly, if the waiting period between the successive scans was short compared to the time needed to thermally empty the filled charge traps, the photocurrent distribution in the gap became more and more uniform with each scan, which could be due to increased carrier lifetime under trap-filled conditions. No photoresponse was observed in the absence of an applied voltage. Figure 7(a) shows photocurrent as a function of applied voltage obtained under *uniform* illumination of the ADT-TIPS-F sample, the scanning photocurrent microscopy data for which were presented in Fig. 6(b). As seen from Fig. 7(a), in this sample the cw photocurrent (I_{cw}) under uniform illumination exhibited quadratic voltage dependence, with $\alpha_{cw}=2.05\pm0.06$. Figures 7(b) and 7(c) show voltage dependencies of the photocurrent obtained under localized excitation of the same sample in the midgap region and in the region near the positively biased electrode, with $\alpha_{cw}=1.2\pm0.2$ and 2.0 ± 0.1, respectively. Clearly, the latter significantly contributed to voltage dependence of the cw photoresponse observed under uniform illumination. Films on Al electrodes typically exhibited stronger dependencies on voltage upon localized excitation of the region close to the positively biased electrode, with $\alpha_{cw}>3$ at higher voltages, also in agreement with those of cw photoresponse under uniform illumination in these samples.

V. DISCUSSION

A. Dark current

1. Samples with Au electrodes

In films on Au electrodes, ohmic response was observed at low voltages, followed by a transition to the space-charge-limited current (SCLC) regime [Fig. 4(a)].[35] Although a hole injection barrier of ~0.25 eV is expected due to the difference between the work function of Au and HOMO energy of our ADT derivatives, this barrier height is low enough to establish SCLC regime in a large range of applied voltages.[39] In Fig. 8(a), the dark current (I_d) data from Fig. 4(a) are replotted as a function of the applied voltage squared (V^2). In the case of the planar electrode geometry used in our experiments, the current flows along a thin layer of unknown thickness, and the current density (j) is expressed in units of A/m (as opposed to A/m^2 for the "sandwich" electrode geometry) and is given by $j=I_d/d$.[40] Although there is no analytical solution for the relationship between SCLC density (j) and voltage (V) in a film of finite thickness on coplanar elec-

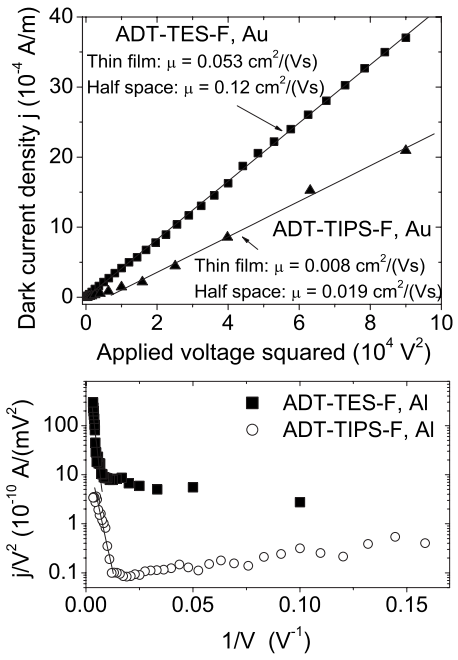

FIG. 8. (a) Dark current density in an ADT-TES-F film on Au 50 μm coplanar and ADT-TIPS-F film on Au 25 μm interdigitated electrodes plotted as a function of applied voltage squared. Fits with Eqs. (1) and (2) are also shown. (b) Dark current density divided by voltage as a function of inverse voltage measured in ADT-TES-F and ADT-TIPS-F films on Al interdigitated electrodes. Fit with FN equation [Eq. (3)] is also included.

trodes, Eqs. (1) and (2) provide solutions for the extreme cases of the infinitely thin film and of the infinite half space, respectively[40]

$$\text{Thin film:} \quad j = \frac{2\mu\epsilon\epsilon_0}{\pi}\frac{V^2}{L^2}, \tag{1}$$

$$\text{Half space:} \quad j = 0.28\mu\epsilon\epsilon_0\frac{V^2}{L^2}. \tag{2}$$

Here ϵ is the relative dielectric constant of the film, ϵ_0 is the dielectric permittivity of vacuum, and L is the gap width between the electrodes (Fig. 2). Using Eqs. (1) and (2), from the slope obtained from a linear fit to the data in Fig. 8(a), and assuming ϵ=3.5, we calculate hole mobilities of μ =0.053 cm^2/(V s) [0.008 cm^2/(V s)] and 0.12 cm^2/(V s) [0.019 cm^2/(V s)] in the approximations of infinitely thin film and infinite half space, respectively, in the ADT-TES-F (ADT-TIPS-F) film. A mobility value in the range of 0.053–0.12 cm^2/(V s) [0.008–0.019 cm^2/(V s)], then, is the lowest hole mobility in the ADT-TES-F (ADT-TIPS-F) film required to account for the observed current. Although mobility values extracted from our SCLC data for the ADT-TES-F film are consistent with those measured in TFT structures in spin-coated ADT-TES-F films on untreated Au electrodes,[10] values as high as 1.5 cm^2/(V s) have been obtained in better-quality ADT-TES-F films, achieved by spin-coating on Au electrodes treated with pentafluorobenzenethiol.[6,8] Therefore, it is likely that the SCLC regime observed in our voltage range is not a trap-filled one, and μ in Eqs. (1) and (2) must be replaced by $\mu_{\text{eff}}=\mu\theta$, where θ is a ratio between the free and trapped charge density ($\theta<1$). This would suggest that the maximum possible SCLC has not been achieved in our samples[35] and that current of higher density can flow in the ADT-TES-F films. Our observation of high cw photocurrents supports this conclusion.[23] Qualitatively, observations discussed above are applicable to ADT-TIPS–F films as well. However, hole mobilities estimated from the SCLC data were lower than those in ADT-TES-F by a factor of 3–8 [e.g., a factor of ~6.6 in Fig. 8(a)], depending on the sample, which is a consequence of different molecular packing in ADT-TES-F and ADT-TIPS-F crystallites and aggregates, as well as of ADT-TIPS-F forming less uniform films and lower-quality interfaces with untreated Au, in comparison to ADT-TES-F.[6,23]

2. Samples with Al electrodes

In samples with Al electrodes, dark current is injection-limited, since potential barriers for both hole and electron injection are high. There is the additional factor of high resistance to current flow through the 2–3 nm thick oxide layer that forms on the aluminum under ambient conditions, and the quantitative contribution of this oxide layer into the observed current-voltage characteristics is currently unknown and requires further investigation. At lower voltages, dark current in films on Al electrodes was at least an order of magnitude smaller than that in similar films on Au electrodes. At higher voltages, a sharp increase in current occurred [Fig. 4(a)], which, in general, can be attributed to several mechanisms, including charge trap filling and Fowler–Nordheim (FN) tunneling.[35] Current-voltage dependencies $I_d \sim V^m$ with $m>7$ were observed in a variety of organic materials and attributed to filling of the traps with exponentially distributed energies.[35,41,42] In most of our samples with Al electrodes, dark current data could indeed be fitted with this power-law function, yielding values of $m>5$, varying from sample to sample. However, if this behavior were due to charge trap filling in the bulk material, large values of m would lead to strong dependence of the current on sample thickness (or, in our case, on the gap width L),[12,35] which was not observed in our experiments. Figure 8(b) shows typical dark current-voltage characteristics obtained in samples with Al electrodes when plotted as the current density (j) divided by the applied voltage (V) as a function of inverse applied voltage ($1/V$). In most samples, the logarithm of (j/V^2) was linear with respect to $1/V$ at higher voltages [Fig. 8(b)], which may suggest charge carrier tunneling through a barrier, described by the FN equation

$$\ln\left(\frac{j}{E^2}\right) = A - \kappa\left(\frac{1}{E}\right), \tag{3}$$

where A is a constant, E is the electric field, and κ is defined by Eq. (4)

$$\kappa = \frac{8\pi\sqrt{2m^*}\Phi_B^{3/2}}{3eh}. \tag{4}$$

Here m^* is the effective carrier mass, h is the Planck constant, and Φ_B is the effective barrier height. In Eq. (4), the barrier lowering due to a Schottky image force has been neglected.

In our case, the electric field E in the FN equation [Eq. (3)] is difficult to quantify. Indeed, in a thin-film device with planar electrode geometry, electric field is not uniformly distributed across the film,[17,18,36] and its distribution depends on various parameters including the gap width between the electrodes, electrode length and width, and film thickness.[12] In dielectric films, the electric field is symmetric with respect to the middle of the gap. When film thickness is much lower than the gap between the electrodes, the field is lowest in the middle of the gap [$E_{\mathrm{mid}}=2V/(\pi L)$], increasing symmetrically toward the electrodes.[18] If the film is semiconducting, however, with one type of carrier more mobile than the other, or with preferred injection and trapping of one carrier type, an asymmetric electric field distribution is produced.[17,18,37,38,47] In particular, one of the electrodes could be screened across a significant portion of the gap by space charge,[17,43] which is compensated in the region close to the other electrode, causing a large change in the potential and a significant increase in electric field in that region. In this case, the electric field at the interface is better described by $E \approx V/L_{\mathrm{eff}}$, where L_{eff} is the effective width, which can be much narrower than the gap width L. The slope of the linear fit of $\ln(j/V^2)$ versus $1/V$ yields a product of κ given by Eq. (4) and L_{eff}. Assuming m^* is equal to the mass of the electron, at $L_{\mathrm{eff}}=L$ [e.g., $L=25$ μm for the data in Fig. 8(b)], the barrier height (Φ_B) value obtained from the fit to, for example, ADT-TES-F data, is only 0.03 eV, which is much lower than 1.15 eV expected solely from the difference between Al work function and HOMO energy of ADT-TES-F in the case of hole tunneling. In order to obtain the barrier height of ~1.15 eV, L_{eff} needs to be about 100 nm. This would be consistent with the width of the depletion region at the injecting contact observed in pentacene films using scanning Kelvin probe force microscopy.[14,44] Most likely, however, the actual barrier height is significantly lower than 1.15 eV, due to disorder of the interfacial states, formation of the interfacial dipole, and barrier lowering due to the image force neglected in Eq. (3).[45–47] Additionally, there is an unknown contribution of the aluminum oxide layer into the properties of the injection barrier.

Although FN tunneling mechanism has been widely used to explain current-voltage characteristics in a variety of organic materials,[48–50] Eq. (3) was derived under assumptions of charge injection in the extended states, and concerns have been expressed in the literature regarding applicability of these assumptions to organic semiconductors.[2,51] In particular, Arkhipov *et al.*[51] showed that if carrier injection into a disordered material is considered, current-voltage dependence at high electric fields can look similar to that due to FN tunneling, and can be explained without invoking a tunneling mechanism. In the model of Ref. 51, which was shown to describe dark currents in a number of systems,[52] energetic disorder in the organic material at the interface promotes charge carrier injection by effectively lowering the barrier. Although voltage dependencies of dark current and cw photocurrent in ADT films on Al electrodes were independent of temperature in the range of 285–330 K at high voltages, which seems to be more consistent with FN mechanism, measurements in the broader temperature range are needed to unambiguously prove validity of either model in the case of ADT-TIPS(TES)-F-Al interfaces.

B. Photocurrent

1. Transient photocurrent

Since measurements of the photocurrent were performed in the presence of applied electric field, the photoresponse was necessarily measured after dark current flow had been established in the film, or, in other words, after the sample had been preconditioned by the dark current. As discussed above, in samples with Au and Al electrodes, very different charge injection conditions obtain, and, therefore, different preconditioning of the samples is realized. In particular, samples with Au electrodes, in which SCLC regime is established, are expected to have a high density of filled hole traps. In contrast, samples with Al electrodes are expected to be in a close-to-pristine condition (empty traps) at low voltages, and have partially filled traps at higher voltages, after hole injection via FN tunneling is enabled. Similar amplitudes of the transient photocurrents obtained in films on Au and Al electrodes [Fig. 3(b)] suggest that the presence of trapped charge carriers, although not negligible, does not play a determining role in charge photogeneration and transport on picosecond time scales. Nevertheless, differences in the initial decay of the transient photocurrent were observed, with films on Al exhibiting a faster initial decay than those on Au [Fig. 3(a)]. Transient photocurrent data obtained in scanning photocurrent microscopy experiments (Sec. IV C) help clarify the nature of this effect: since differences in the initial decay in the films on Au and Al electrodes were observed upon excitation of *any* region in the gap, including that far away from the electrodes, fast initial decay is related to bulk material properties and is most likely due to fast trapping of photogenerated holes.[7,20,21,32] In films on Au electrodes, many hole traps are prefilled by dark current, which reduces density of empty traps, which in turn reduces initial trapping of the photogenerated holes. In contrast, most traps in films on Al electrodes are empty and are readily filled by photogenerated holes, thus leading to a fast initial decay of the photocurrent. This would be consistent with previously observed slowing down of the initial decay of the transient photocurrent upon increasing applied electric field in ADT-TIPS-F films on Al electrodes.[7]

2. Cw photocurrent

In contrast to transient photocurrent, photoresponse under cw illumination is strongly affected by the conditions imposed by the electrode material [Fig. 4(b)]. The steady-state photocurrent (I_{cw}) in the case of a homogeneous photoconductor is proportional to the photoconductive gain (G), which is the ratio of the number of charge carriers generated by photoexcitation passing through a solid between two electrodes to the number of quanta absorbed by this solid during the same period of time.[11] The photoconductive gain is strongly influenced by the type of the photoconductor, depending on relative hole and electron mobilities and on whether the carriers can be replenished at the electrodes. In

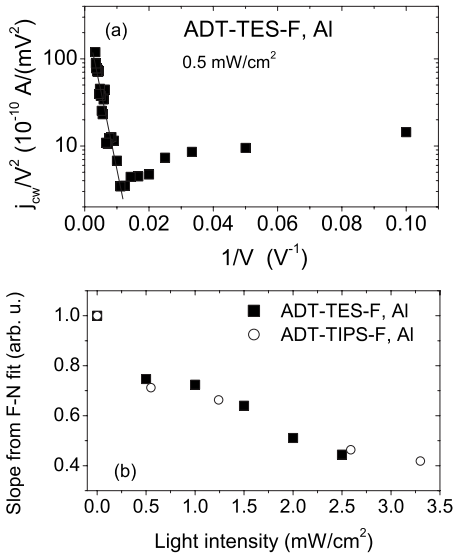

FIG. 9. (a) Photocurrent density divided by applied voltage as a function of inverse voltage measured in an ADT-TES-F film on coplanar Al electrodes with cw photoexcitation at 0.5 mW/cm^2. Fit with FN equation [Eq. (3)] is also shown. (b) Slope from FN fits [Eq. (3)] to the cw photocurrent data (which reflects the product of the barrier height Φ_B and effective width L_{eff}), normalized at its value for the case of dark current (at $I=0$), as a function of light intensity I in ADT-TES-F and ADT-TIPS-F films.

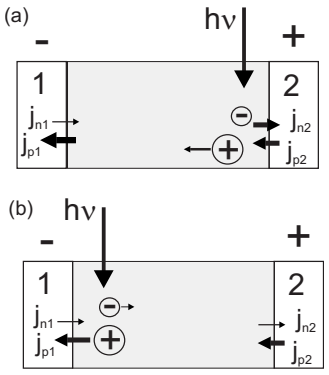

FIG. 10. Schematics of the cw photoresponse under localized excitation of the region near (a) positively and (b) negatively biased electrodes. $j_{n1,2}$ ($j_{p1,2}$) are electron (hole) currents flowing across the metal-organic interfaces at the electrodes 1 and 2, respectively.

the case of dominant hole transport, $G \approx \eta_0 \tau / t_{\text{tr}}$, where τ is a carrier lifetime and t_{tr} is the transit time for a hole to travel across the sample. The photoconductive gain G can be much larger than the initial photogeneration efficiency η_0,[23,53] provided holes are efficiently replenished at the electrodes, which is the case of ADT films on Au electrodes.[11] This is in contrast to samples with non-injecting electrodes, such as ADT films on Al electrodes at low voltages, in which the maximal achievable gain cannot exceed η_0.[11,23,33]

In Fig. 9(a), cw photocurrent (linear) density j_{cw}, obtained in ADT-TES-F film on Al electrodes, divided by applied voltage squared (i.e., j_{cw}/V^2), is plotted as a function of inverse voltage $(1/V)$. Interestingly, the behavior of the photocurrent in samples with Al electrodes is similar to that of the dark current and is consistent with FN tunneling.[54] The product of the barrier height Φ_B and effective gap width L_{eff}, calculated from the FN fit [Eq. (3)] to the photocurrent data, is lower than that obtained for the dark current, and it decreases as the light intensity increases [Fig. 9(b)]. This suggests that photogenerated electrons trapped near the positively biased electrode increase electric field in this region (thus reducing L_{eff}). It also indicates that at higher voltages, once FN tunneling is enabled, the electrode begins to effectively replenish holes, increasing the photoconductive gain G. As a result, at high voltages the photocurrent values in samples with Al electrodes start rapidly approaching those achieved in samples with Au electrodes [Fig. 4(b)].

Additional insight is provided by comparison of the photoresponse profiles obtained by photocurrent scanning microscopy, in particular: (i) amplitudes of transient photocurrents versus cw photocurrents (Figs. 5 and 6, respectively) and (ii) cw photocurrents in samples with Al versus Au electrodes [Figs. 6(a) and 6(b)], respectively). Clearly, the degree of asymmetry with respect to the middle of the gap, as well as the difference between photocurrent profiles in films on Au and Al electrodes, are much more pronounced in the case of cw photocurrent, compared to transient. This is expected, since the amplitudes of the transient photocurrent are proportional to the number of photogenerated carriers immediately after photoexcitation, whereas steady-state photocurrent measured under cw illumination is proportional to the number of the photogenerated carriers reaching the electrodes.[27,31] In order to maintain steady-state photocurrent, the continuity condition $|j_{n1}|+|j_{p1}|=|j_{n2}|+|j_{p2}|$, where $j_{n1,2}$ ($j_{p1,2}$) are electron (hole) currents flowing across the metal-organic interfaces at electrodes 1 and 2, respectively (Fig. 10), must be met.[27,31] Our observation of the maximum cw photocurrent produced upon excitation of a region close to the positively biased electrode, regardless of the electrode material, is a reflection of the fact that holes are more mobile than the electrons in ADT films,[17,31] as illustrated in Fig. 10. In samples with either Au or Al electrodes, electron injection is negligible, and thus $j_{n1} \approx 0$. When the region close to the positive electrode 2 is illuminated, current due to photogenerated holes reaching electrode 1 (j_{p1}) must be balanced by currents due to photogenerated electrons entering electrode 2 (j_{n2}) and due to holes injected from electrode 2 (j_{p2}), i.e., $|j_{p1}| \approx |j_{n2}|+|j_{p2}|$ [Fig. 10(a)]. If electrons are much less mobile than holes, then only electrons that are generated very close to the contact [within several micrometers, according to Fig. 6(a)] reach the electrode, thus producing nonzero current j_{n2}. If the film is illuminated away from the positively biased contact, then $j_{n2} \approx 0$, and the current j_{p1} is limited by the injected hole current j_{p2}, which is high in samples with Au electrodes and low in samples with Al electrodes (at voltages below those at which efficient FN tunneling occurs). This qualitatively explains a much sharper photocurrent dropoff in the sample with Al electrodes compared to that with Au electrodes, as photoexcitation is moved from the positive electrode toward the midgap (Fig. 6). When the region close to negatively biased electrode 1 is illuminated [Fig. 10(b)], a large current due to photogenerated holes entering electrode 1 (j_{p1}) must be balanced by the hole injection current j_{p2}, since in this case $j_{n1} \approx j_{n2} \approx 0$ in samples with either Au or Al electrodes (i.e., $|j_{p1}| \approx |j_{p2}|$). As a result, measurable currents are observed in films on Au electrodes,

in which hole injection is efficient, in contrast to those on Al electrodes, in which $|j_{p2}|$ is low. Although this simple description provides qualitative explanation for the observed behavior, electric field changes due to trapped photogenerated charge carriers, which affect further charge photogeneration, transport and trapping need to be taken in to account, in order to quantitatively explain the profiles in Fig. 6. In particular, voltage dependence of the photocurrent measured under localized photoexcitation depends on the location of photoexcitation in the gap (as illustrated in Fig. 7) and is determined by the electric field distribution in the gap, as well as by electric field dependencies of the contributing currents (in our case j_{p1}, j_{p2}, and j_{n2}) and their relative magnitudes.

VI. CONCLUSIONS

In summary, we examined contribution of effects at metal-organic interfaces to photoresponse in functionalized ADT thin films. On picosecond time scales, fast photoresponse due to photogenerated holes moving under applied voltage was comparable in films on Au and Al electrodes. In samples with Au electrodes, fast initial decay of the transient photocurrent was not as pronounced as in those with Al electrodes, due to high density of traps filled by holes injected from the Au electrode, which reduced initial trapping of photogenerated holes. The slower decay component, which lasted up to at least microsecond time scales, was not significantly affected by the trapped charge carriers.

In ADT films on Au electrodes, dark current and cw photocurrent were higher by more than an order of magnitude than those in similar films on Al electrodes. While space-charge-limited currents were observed in samples on Au electrodes, injection-limited currents at low applied voltages, with a transition consistent with FN tunneling at higher voltages, were obtained in samples on Al electrodes. FN tunneling was also observed in cw photoresponse of films on Al electrodes.

Photocurrent profiles, obtained in ADT films on coplanar electrodes by photocurrent scanning microscopy, revealed differences in the distribution across the gap of (i) transient photocurrent amplitudes versus cw photocurrent and (ii) cw photocurrents in samples with Au and Al electrodes. These observations supported results obtained in the same devices under uniform illumination.

ACKNOWLEDGMENTS

We thank Professor Y.-S. Lee and J. Tomaino for technical support. This work was supported in part by the Petroleum Research Fund, Office of Naval Research (Grant No. N00014-07-1-0457) via ONAMI Nanometrology and Nanoelectronics Initiative, and National Science Foundation via CAREER (Program No. DMR-0748671).

[1]W. Brutting, *Physics of Organic Semiconductors* (Wiley-VCH, Weinheim, 2005).
[2]J. C. Scott, J. Vac. Sci. Technol. A **21**, 521 (2003).
[3]Y. Shen, A. R. Hosseini, M. H. Wong, and G. G. Malliaras, ChemPhysChem **5**, 16 (2004).
[4]J. E. Anthony, Chem. Rev. (Washington, D.C.) **106**, 5028 (2006).
[5]S. K. Park, T. N. Jackson, J. E. Anthony, and D. A. Mourey, Appl. Phys. Lett. **91**, 063514 (2007).
[6]S. Subramanian, S. K. Park, S. R. Parkin, V. Podzorov, T. N. Jackson, and J. E. Anthony, J. Am. Chem. Soc. **130**, 2706 (2008).
[7]J. Day, S. Subramanian, J. E. Anthony, Z. Lu, R. J. Twieg, and O. Ostroverkhova, J. Appl. Phys. **103**, 123715 (2008).
[8]S. K. Park, D. A. Mourey, S. Subramanian, J. E. Anthony, and T. N. Jackson, Appl. Phys. Lett. **93**, 043301 (2008).
[9]D. J. Gundlach, J. E. Royer, S. K. Park, S. Subramanian, O. D. Jurchescu, B. H. Hamadani, A. J. Moad, R. J. Kline, L. C. Teague, O. Kirillov, C. A. Richter, J. G. Kushmerick, L. J. Richter, S. R. Parkin, T. N. Jackson, and J. E. Anthony, Nature Mater. **7**, 216 (2008).
[10]O. D. Jurchescu, B. H. Hamadani, H. D. Xiong, S. K. Park, S. Subramanian, N. M. Zimmerman, J. E. Anthony, T. N. Jackson, and D. J. Gundlach, Appl. Phys. Lett. **92**, 132103 (2008).
[11]K. C. Kao, *Dielectric Phenomena in Solids* (Elsevier, New York, 2004).
[12]M. A. Lampert and P. Mark, *Current Injection in Solids* (Academic, New York, 1970).
[13]M. Brinza, J. Willekens, M. L. Benkhedir, E. V. Emelianova, and G. J. Andriaenssens, J. Mater. Sci. Mater. Electron. **16**, 703 (2005).
[14]K. P. Puntambekar, P. V. Pesavento, and C. D. Frisbie, Appl. Phys. Lett. **83**, 5539 (2003).
[15]S. Barth, H. Bassler, H. Rost, and H. H. Horhold, Phys. Rev. B **56**, 3844 (1997).
[16]D. Ray, M. P. Patankar, N. Periasamy, and K. L. Narasimhan, J. Appl. Phys. **98**, 123704 (2005).
[17]T. Agostinelli, M. Caironi, D. Natali, M. Sampietro, P. Biagioni, M. Finazzi, and L. Duo, J. Appl. Phys. **101**, 114504 (2007).
[18]D. D. Nolte, N. P. Chen, M. R. Melloch, C. Montemagno, and N. M. Haegel, Appl. Phys. Lett. **68**, 72 (1996).
[19]O. Ostroverkhova and W. E. Moerner, Chem. Rev. (Washington, D.C.) **104**, 3267 (2004).
[20]O. Ostroverkhova, D. G. Cooke, S. Shcherbyna, R. F. R. F. Egerton, F. A. Hegmann, R. R. Tykwinski, and J. E. Anthony, Phys. Rev. B **71**, 035204 (2005).
[21]O. Ostroverkhova, S. Shcherbyna, D. G. Cooke, R. F. Egerton, F. A. Hegmann, R. R. Tykwinski, S. R. Parkin, and J. E. Anthony, J. Appl. Phys. **98**, 033701 (2005).
[22]J. S. Brooks, T. Tokumoto, E. S. Choi, D. Graf, N. Biskup, D. L. Eaton, J. E. Anthony, and S. A. Odom, J. Appl. Phys. **96**, 3312 (2004).
[23]A. D. Platt, J. Day, S. Subramanian, J. E. Anthony, and O. Ostroverkhova (unpublished).
[24]J. Day, A. D. Platt, O. Ostroverkhova, S. Subramanian, and J. E. Anthony, Appl. Phys. Lett. **94**, 013306 (2009).
[25]D. Moses, C. Soci, P. Miranda, and A. J. Heeger, Chem. Phys. Lett. **350**, 531 (2001).
[26]C. Im, E. V. Emelianova, H. Bassler, H. Spreitzer, and H. Becker, J. Chem. Phys. **117**, 2961 (2002).
[27]Y. Gu, E. S. Kwak, J. L. Lensch, J. E. Allen, T. W. Odom, and L. J. Lauhon, Appl. Phys. Lett. **87**, 043111 (2005).
[28]E. J. H. Lee, K. Balasubramanian, R. T. Weitz, M. Burghard, and K. Kern, Nat. Nanotechnol. **3**, 486 (2008).
[29]E. J. H. Lee, K. Balasubramanian, J. Dorfmuller, R. Vogelgesang, N. Fu, A. Mews, M. Burghard, and K. Kern, Small **3**, 2038 (2007).
[30]T. F. Carruthers, J. F. Weller, S. C. Binari, and P. E. Thompson, IEEE Elec. Dev. Lett. **EDL-3**, 347 (1982).
[31]Y. Gu, J. P. Romankiewicz, J. K. David, J. L. Lensch, and L. J. Lauhon, Nano Lett. **6**, 948 (2006).
[32]O. Ostroverkhova, D. G. Cooke, F. A. Hegmann, J. E. Anthony, V. Podzorov, M. E. Gershenson, O. D. Jurchescu, and T. T. M. Palstra, Appl. Phys. Lett. **88**, 162101 (2006).
[33]T. K. Daubler, D. Neher, H. Rost, and H. H. Horhold, Phys. Rev. B **59**, 1964 (1999).
[34]A. Rose, *Concepts in Photoconductivity and Allied Problems* (Interscience, New York, 1963).
[35]M. Pope and C. E. Swenberg, *Electronic Processes in Organic Crystals and Polymers* (Oxford University Press, New York, 1999).
[36]S. J. Hwang, H. H. Silveira, and J. Wang, Opt. Commun. **233**, 341 (2004).
[37]J. D. Slinker, J. A. DeFranco, M. J. Jaquith, W. R. Silveira, Y. W. Zhong, J. M. Moran-Mirabal, H. G. Craighead, H. D. Abruna, J. A. Marohn, and G. G. Malliaras, Nature Mater. **6**, 894 (2007).
[38]T. Manaka, M. Nakao, D. Yamada, E. Lim, and M. Iwamoto, Opt. Express **15**, 15964 (2007).
[39]F. Neumann, Y. A. Genenko, C. Melzer, S. V. Yampolskii, and H. von

Seggern, Phys. Rev. B **75**, 205322 (2007).
[40]W. Hu, B. Gompf, J. Pflaum, D. Schweitzer, and M. Dressel, Appl. Phys. Lett. **84**, 4720 (2004).
[41]A. J. Campbell, M. S. Weaver, D. G. Lidzey, and D. D. C. Bradley, J. Appl. Phys. **84**, 6737 (1998).
[42]M. A. Baldo and S. R. Forrest, Phys. Rev. B **64**, 085201 (2001).
[43]C. M. Hurd and W. R. McKinnon, J. Appl. Phys. **75**, 596 (1994).
[44]J. A. Nichols, D. J. Gundlach, and T. N. Jackson, Appl. Phys. Lett. **83**, 2366 (2003).
[45]B. H. Hamadani and D. Natelson, J. Appl. Phys. **97**, 064508 (2005).
[46]L. Diao, C. D. Frisbie, D. D. Schroepfer, and P. P. Ruden, J. Appl. Phys. **101**, 014510 (2007).
[47]T. N. Ng, W. R. Silveira, and J. A. Marohn, Phys. Rev. Lett. **98**, 066101 (2007).
[48]R. Blum, M. Sprave, J. Sablotny, and M. Eich, J. Opt. Soc. Am. B **15**, 318 (1998).
[49]V. Burtman, Thin Solid Films **516**, 3436 (2008).
[50]J. Chen and D. Ma, Chem. Phys. **325**, 225 (2006).
[51]V. I. Arkhipov, E. V. Emelianova, Y. H. Tak, and H. Bassler, J. Appl. Phys. **84**, 848 (1998).
[52]T. van Woudenbergh, J. Wildeman, and P. W. M. Blom, Phys. Rev. B **71**, 205216 (2005).
[53]J. Gao and F. A. Hegmann, Appl. Phys. Lett. **93**, 223306 (2008).
[54]T. Katsume, M. Hiramoto, and M. Yokoyama, Appl. Phys. Lett. **69**, 3722 (1996).